Electron Spin-Vorticity Coupling in Pipe Flows at Low and High Reynolds Number

Hamid Tabaei Kazerooni,[*] Alexander Thieme,[†] Jörg Schumacher,[‡] and Christian Cierpka[§]
Institute of Thermodynamics and Fluid Mechanics, Technische Universität Ilmenau, Ilmenau 98684, Germany

(Received 7 February 2020; revised 8 April 2020; accepted 5 June 2020; published 1 July 2020)

Spin-hydrodynamic coupling is a recently discovered method to directly generate electricity from an electrically conducting fluid flow in the absence of Lorentz forces. This method relies on a collective coupling of electron spins—the internal quantum-mechanical angular momentum of the electrons—with the local vorticity of a fluid flow. In this work, we experimentally investigate the spin-hydrodynamic coupling in circular- and noncircular-capillary pipe flows and extend a previously obtained range of Reynolds numbers to smaller and larger values, $20 < \mathrm{Re} < 21\,500$, using the conducting liquid-metal alloy (Ga,In)Sn as the working liquid. In particular, we provide experimental evidence for the linear dependence of the generated electric voltage with respect to the bulk-flow velocity in the laminar regime of the circular pipe flow as predicted by Matsuo *et al.* [Phys. Rev. B. **96**, 020401 (2017)]. Moreover, we show analytically that this behavior is universal in the laminar regime regardless of the cross-sectional shape of the pipe. Finally, the proposed scaling law by Takahashi *et al.* [Nat. Phys. **12**, 52 (2016)] for the generated voltage in turbulent circular pipe flows is experimentally evaluated at Reynolds numbers higher than in previous studies. Our results verify the reliability of the proposed scaling law for Reynolds numbers up to $\mathrm{Re} = 21\,500$ for which the flow is in a fully developed turbulent state.

DOI: 10.1103/PhysRevApplied.14.014002

I. INTRODUCTION

Fluid-dynamical processes in connection with quantum many-body phenomena are known from quantum turbulence at low temperatures close to absolute zero [1,2] and strongly correlated electron systems in graphene that resemble the transport properties of a classical viscous fluid [3], to mention two prominent examples for bosonic and fermionic systems, respectively. Besides the electric charge, an electron carries an intrinsic angular momentum known as electron spin—or, in short, spin. Over the past 30 years, this fundamental quantum property of an electron has spawned a multidisciplinary research field called spintronics, analogous to electronics [4]. The ultimate goal of spintronics is to exploit the electron spins along with their charges to fabricate more efficient, faster, and smaller devices for data processing and storage. In this context, as for the charge current in conventional electronic devices, the generation and manipulation of the flow of electron spins, i.e., the spin current, are the main tasks in spintronics [5,6]. However, these are very challenging to realize as, unlike the charge current, the spin current is not a conserved quantity. Nevertheless, different approaches have been proposed to drive the spin current, mainly based on angular-momentum exchange between the electron spin and other physical entities such as light polarization [7] and magnetization [8]. Uchida *et al.* [9] have shown that a temperature gradient can also induce a spin current in a metallic magnet, i.e., the spin Seebeck effect.

Recently, Takahashi *et al.* [10] investigated spin-current generation through a direct coupling between electron spins and the microscopic rotation of a material system as the most well-known form of angular momentum [11]. In particular, they utilized the vorticity generated by turbulent flows of liquid metals in narrow circular pipes as a source of mechanical rotation. In a fluid flow, vorticity is a measure of the local rotation of a fluid element and it is mathematically defined as $\boldsymbol{\omega} = \boldsymbol{\nabla} \times \mathbf{u}$, where $\mathbf{u} = (u_x, u_y, u_z)$ is the three-dimensional flow-velocity field. Takahashi *et al.* [10] argued that the electron spins are polarized in the direction of the flow vorticity due to the spin-mechanical angular-momentum coupling. Moreover, they showed that the gradient of the vorticity results in a spin-voltage gradient and consequently a spin current in the direction of the vorticity gradient. It has been found that a spin current induces an electric current transversal

[*]hamid.kazerooni@tu-ilmenau.de
[†]alexander.thieme@tu-ilmenau.de
[‡]joerg.schumacher@tu-ilmenau.de
[§]christian.cierpka@tu-ilmenau.de

to the spin-current direction due to the spin-orbit interaction [12]. This phenomenon is known as the inverse spin Hall effect (ISHE) (see Saitoh *et al.* [13]) and has been employed by Takahashi *et al.* [10] to detect the induced charge current as a faint voltage V_{ISHE} signal in the flow direction of a turbulent pipe flow where the mean vorticity changes along the radial direction [14]. Based on a theoretical analysis, they have also predicted that the voltage V_{ISHE}, which is measured along the pipe flow direction, should be mainly proportional to the square of the turbulent friction velocity u_τ in a circular pipe flow and that its magnitude is of the order of nanovolts. Their experimental results are in very good agreement with their theoretical prediction using mercury (Hg) and the eutectic alloy made of gallium, indium, and tin [(Ga,In)Sn] as working liquids. Subsequently, Matsuo *et al.* [15] have shown theoretically that the voltage V_{ISHE} increases linearly with respect to the bulk-flow velocity U_b in laminar circular pipe flows. However, they have not provided any experimental evidence for this claim. It is one of the main motivations of the present study to fill this gap and to verify the voltage generation in an independent experimental setup that we will present in the following.

To do so, we design and develop an experimental apparatus that allows us to measure the generated voltage V_{ISHE} in both the laminar and the turbulent regimes and thus to extend the range of previously obtained flow Reynolds numbers. Our measurements are performed using circular-capillary tubes with diameters D ranging from 0.1 mm to 1.2 mm for a wide range of Reynolds numbers $\mathrm{Re} = U_b D/\nu$ from 20 to 21 500, where U_b and $\nu = 3.3 \times 10^{-7}\,\mathrm{m^2\,s^{-1}}$ are the bulk-flow velocity and the kinematic viscosity of (Ga,In)Sn as the working liquid, respectively. The (Ga,In)Sn eutectic alloy is used due to its low kinematic viscosity, low melting temperature (10.5 °C) and, importantly, its low toxicity.

The present experiments extend the previous measurements of Takahashi *et al.* [10] in two directions. (1) Our results show that the generated voltage $V_{\mathrm{ISHE}}^{\mathrm{lam}}$, as predicted by Matsuo *et al.* [15], is linearly proportional to the bulk-flow velocity U_b in the laminar regime. To better understand the role of the capillary-tube cross-sectional shape on the spin-hydrodynamic coupling, measurements are also carried out in a rectangular capillary tube and the laminar flow regime. (2) In the turbulent regime, we investigate the generated voltage $V_{\mathrm{ISHE}}^{\mathrm{turb}}$ at four times higher Reynolds numbers than in previous studies, which have been limited to $\mathrm{Re} < 5000$ using (Ga,In)Sn as the working liquid. This brings us into the fully developed regime of pipe-flow turbulence. Our work is an independent confirmation of the measurements of Takahashi *et al.* [10]. We find very good agreement with their data for the same range of Reynolds numbers and with (Ga,In)Sn as the working liquid. Moreover, the results of the present study provide strong evidence for an extended validity of the universal scaling law proposed by Takahashi *et al.* [10] for flows at high Reynolds numbers.

II. EXPERIMENTAL SETUP

The experimental setup is designed to investigate the spin-hydrodynamic coupling and to measure the related generated electric voltage V_{ISHE} produced by laminar and turbulent flows of (Ga,In)Sn in different capillary tubes. Figure 1 shows a schematic illustration of the apparatus, which comprises a pressurized feeding vessel (2) and a collecting container (4), both made of plexiglass, a capillary tube (3), a weight scale (5) for estimating the liquid-metal flow rate, and several sensors for monitoring the temperature (7) and measuring the longitudinal generated voltage V_{ISHE} (6). To conduct experiments, the liquid metal is loaded into the top-sealed vessel with a total volume of 63 ml. The flow is driven to the capillary tube using pressurized argon gas. A precise weight scale (Sartorius AG) is used to measure the weight change of the collecting container in order to accurately calculate the flow rate and the corresponding bulk-flow velocity U_b based on the (Ga,In)Sn density $\rho = 6330\ \mathrm{kg/m^3}$ and the measurement time. Table I presents all the physical properties of the (Ga,In)Sn alloy used in this study and taken from Plevachuk *et al.* [16] and Eckert [17]. It is known that the surface of (Ga,In)Sn can be easily oxidized in the presence of air. This effect is minimized using the noble gas argon to pressurize the liquid metal and generate the flow. Nevertheless, a layer of oxide forms on the surface of the liquid metal in the top and bottom vessels. It is worth mentioning

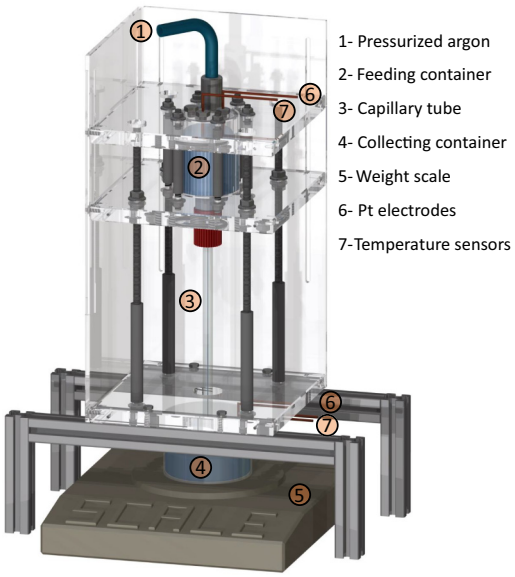

FIG. 1. A schematic illustration of the employed experimental setup for measuring the inverse spin Hall voltage V_{ISHE} generated by laminar and turbulent flows in different narrow-capillary tubes.

TABLE I. A list of the material properties of (Ga,In)Sn at 26 °C taken from Ref. [16]. The value of the specific heat at constant pressure c_p, which is required to calculate κ, is obtained by extrapolation from data at higher temperatures [17].

Physical quantity	Value (SI units)
Mass density	$\rho = 6330\ \mathrm{kg/m^3}$
Kinematic viscosity	$\nu = 3.30 \times 10^{-7}\ \mathrm{m^2/s}$
Thermal diffusivity	$\kappa = 1.1 \times 10^{-5}\ \mathrm{m^2/s}$
Magnetic diffusivity	$\beta = 0.24\ \mathrm{m^2/s}$
Electrical conductivity	$\sigma_0 = 3.26 \times 10^6\ (\Omega\,\mathrm{m})^{-1}$

that these oxide layers remain unperturbed at the surface and they are not mixed with the whole liquid during the experiment.

Capillary tubes with different diameters, lengths, and cross sections can be easily mounted via different adapters to the system. The majority of the measurements are carried out using capillary tubes made of borosilicate glass (Hilgenberg GmbH) with a circular cross section and different diameters of $D = 0.1$, 0.4, 0.8 and 1.2 mm to cover a wide range of Reynolds numbers Re. In order to investigate the effect of the capillary-tube cross-sectional shape on the spin-hydrodynamic coupling in the laminar regime, additional measurements are performed using a rectangular capillary tube with a sectional dimension of $W \times H = 0.334 \times 0.149\ \mathrm{mm^2}$ and a hydraulic diameter of $D_{h_{\mathrm{Rec}}} = 2WH/(W+H) = 0.2$ mm. For the sake of comparability, the length of all capillaries is chosen to be $L = 200$ mm. The generated voltage V_{ISHE} is measured by means of a nanovoltmeter (Keithley 2182A) and two very thin wires ($d = 0.4$ mm) made of platinum (Pt) implemented in the top and bottom vessels as electrodes. The liquid (Ga,In)Sn in the top vessel is connected to ground to prevent the accumulation of static electric charge. The temperature of the vessels is also monitored using calibrated PT100 resistance thermometers with an uncertainty of ±0.1 °C. The whole apparatus is placed inside a thermally controlled chamber and the system is operated for a few hours before each set of experiments to reach stable conditions at 26 °C. Nevertheless, temperature differences may occur due to the argon-gas compression and expansion in the setup. Considering the upper vessel height $L = 50$ mm and the thermal diffusivity κ of (Ga,In)Sn from Table I, the diffusion time, $\tau = L^2/\kappa$, of the heat in the upper vessel can be roughly estimated to be about 200 s. To minimize thermal effects in the system, measurements are only carried out with a fully filled vessel and for a time duration of 10 s. Data acquisition is carried out using the National Instruments LabVIEW™ software package. The sampling frequency is set to 2 Hz, corresponding to a maximum resolution of 1 nV for recording the generated voltage V_{ISHE} via the nanovoltmeter.

III. THEORETICAL ASPECTS

As mentioned before, Takahashi *et al.* [10] were the first to discover and introduce the concept of spin-hydrodynamic generation. Besides the experimental evidence, they also provided a theoretical framework to explain this phenomenon. In short, based on the angular-momentum conservation law in fluid flow and the spin-diffusion equation, they proposed an equation to describe the relationship between the vectorial spin voltage $\boldsymbol{\mu}^S$ and the flow vorticity $\boldsymbol{\omega}$ vector. This extension of the Valet-Fert equation for spin diffusion [18] reads as follows:

$$\nabla^2 \boldsymbol{\mu}^S = \frac{1}{\lambda^2}\boldsymbol{\mu}^S - \frac{4e^2\xi}{\sigma_0 \hbar}\boldsymbol{\omega}, \tag{1}$$

where λ, e, $\hbar$, and σ_0 are the spin-diffusion length, the elementary charge, the reduced Planck constant, and the electrical conductivity of the liquid metal, respectively. Takahashi *et al.* [10] defined ξ as a parameter that represents the angular-momentum transfer from the fluid into electron spins. They also argued that ξ is different for laminar ξ_{lam} and turbulent ξ_{turb} flows. Note that the vector notation in Eq. (1) indicates the polarization direction of the spin voltage $\boldsymbol{\mu}^S$, which corresponds to the flow-vorticity direction. For more details on the derivation of Eq. (1), see Takahashi *et al.* [10]. It is also shown that the induced spin current $\mathbf{j}^S$ and the electric field $\mathbf{E}_{\mathrm{ISHE}}$ due to the ISHE can be described as

$$\mathbf{E}_{\mathrm{ISHE}} = -\frac{2|e|}{\sigma_0 \hbar}\theta_{\mathrm{SHE}}\, \mathbf{j}^S \times \boldsymbol{\sigma}, \tag{2}$$

where θ_{SHE} and $\boldsymbol{\sigma}$ are the spin Hall angle and the spin-polarization vector [13]. Hence, the charge current can be written as $j_i^C = -\frac{2|e|}{\hbar}\theta_{\mathrm{SHE}}\epsilon_{ijk}j_{jk}^S$ using the Levi-Civita symbol ϵ_{ijk} in tensor notation. It is well known that the average streamwise velocity profile in a wall-bounded pressure-driven turbulent flow close to the wall in the viscous sublayer δ_0 is a linear function of the wall-normal direction y and reads as follows:

$$\frac{\overline{u_z}(y)}{u_\tau} = \frac{y u_\tau}{\nu}, \tag{3}$$

where $u_\tau = \sqrt{\tau_w/\rho}$ is the turbulent friction velocity, in which τ_w and ρ are the wall-shear stress and the fluid density, respectively. It is also well accepted that the log law describes the velocity profile away from the viscous sublayer along the wall-normal direction y in canonical flows as follows [19]:

$$\frac{\overline{u_z}(y)}{u_\tau} = \frac{1}{\kappa_+}\ln\left(\frac{y u_\tau}{\nu}\right) + B, \tag{4}$$

where κ_+ and B are the von Kármán constant and the additive coefficient, respectively. Takahashi *et al.* [10]

have employed the above velocity profile with $\kappa_+ \approx 0.41$ and $B \approx 5.5$ to calculate the vorticity field in a turbulent pipe flow with a circular cross section in cylindrical coordinates.

Figure 2(a) shows the mean-flow-velocity profile, the corresponding mean vorticity field, and its gradient for a turbulent circular pipe flow in cylindrical coordinates, with z being the streamwise and r the wall-normal direction, respectively. Clearly, the mean vorticity field $\boldsymbol{\omega}$ of a circular pipe flow consists of only one component in the azimuthal θ direction $\omega_\theta(r) = -\partial_r \overline{u_z}(r)$. Based on Eq. (2), the gradient of the vorticity and consequently the spin voltage in the radial direction, $\partial \mu_\theta^S(r)/\partial r \propto \partial \omega_\theta(r)/\partial r$, is responsible for inducing the charge current along the streamwise direction j_z^C. Hence, the mean vorticity in the viscous sublayer $\omega_\theta(r) = u_\tau^2/\nu$ does not contribute to the spin-hydrodynamic generation, as its radial gradient is zero. However, the radial-vorticity gradient in the log-law region is not constant and can be expressed as

$$\frac{\partial \omega_\theta(r)}{\partial r} = \frac{u_\tau}{\kappa_+} \frac{1}{(r_0 - r)^2}. \tag{5}$$

Therefore, the radial-vorticity gradient in the log-law region, especially close to the wall where it is more significant, is the main source of the induced spin and charge current in the same r and the transversal z direction, respectively [see Fig. 2(a)]. Note that here the wall-normal direction in a Cartesian coordinate is transformed into the cylindrical one using $y = r - r_0$, where r_0 is the pipe radius. Takahashi [10] employed Eq. (5) and analytically solved Eqs. (1) and (2) for a turbulent pipe flow with a circular cross section. For the sake of simplicity, they neglected the buffer layer between the viscous sublayer and the log-law region. Based on their analysis, Takahashi *et al.* [10] proposed a universal scaling law for the inverse spin Hall voltage $V_{\mathrm{ISHE}}^{\mathrm{turb}}$ generated in a turbulent circular pipe flow as a nonlinear function of the turbulent friction velocity u_τ:

$$\frac{r_0^3 V_{\mathrm{ISHE}}^{\mathrm{turb}}}{L} = \left(\frac{4|e|}{\hbar}\right)\left(\frac{\theta_{\mathrm{SHE}} \lambda^2 \xi_{\mathrm{turb}}}{\sigma_0}\right)\left(\frac{1}{\kappa_+}\right) \times \left[\frac{(u_\tau r_0)^2}{\nu \mathrm{Re}_\tau^{\delta_0}} - (u_\tau r_0) \ln \frac{(u_\tau r_0)}{\nu \mathrm{Re}_\tau^{\delta_0}} - (u_\tau r_0)\right], \tag{6}$$

where $\mathrm{Re}_\tau^{\delta_0} = u_\tau \delta_0/\nu \approx 11.6$ is the friction Reynolds number based on the viscous sublayer thickness δ_0. Note that this value for $\mathrm{Re}_\tau^{\delta_0}$ can be achieved when one considers the viscous sublayer thickness as the height, $y = r_0 - r$, at which the logarithmic velocity profile [see Eq. (4)] intersects with the linear velocity profile of the viscous sublayer [see Eq. (3)]. A series of experimental measurements by Takahashi *et al.* [10] have shown the reliability of the proposed scaling law in a range of Reynolds number Re from 4000 to 10 000, using Hg as the working liquid.

The same procedure as described above has been followed by Matsuo *et al.* [15] to obtain a universal scaling for the generated voltage V_{ISHE} in a laminar circular pipe flow with a parabolic velocity profile, as

$$u_z(r) = 2U_b\left[1 - \left(\frac{r}{r_0}\right)^2\right]. \tag{7}$$

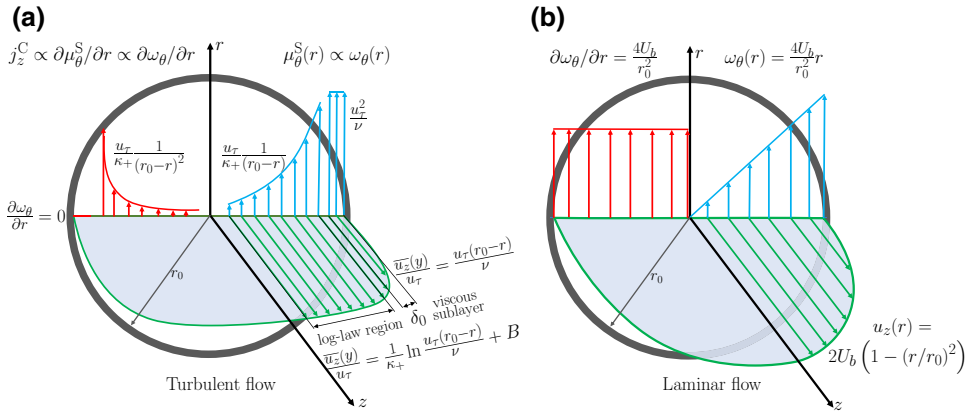

FIG. 2. (a) The turbulent circular pipe-flow mean velocity (green profile), the mean vorticity field (blue profile), and the mean radial-vorticity gradient (red profile). The electron spins are aligned along the mean vorticity direction. The spin voltage is proportional to the mean flow vorticity $\mu_\theta^S(r) \propto \omega_\theta(r)$. The radial gradient of the spin voltage due to the change of the flow vorticity along the pipe radius induces charge current in the streamwise direction, based on the inverse spin Hall effect (ISHE) $j_z^C \propto \partial\mu_\theta^S/\partial r \propto \partial\omega_\theta/\partial r$. The gap between the viscous sublayer and the log-law region, which is called the buffer layer, is neglected by Takahashi *et al.* [10] in their analysis. (b) The parabolic velocity profile (green) of a laminar circular pipe flow and the corresponding vorticity field (blue profile) and constant radial-vorticity gradient (red profile). The vectors in these figures are only for illustration purposes and are not scaled based on the magnitude of each quantity.

As shown in Fig. 2(b), the vorticity field again has only one component, $\omega_\theta(r) = 4U_b r/r_0^2$, in the azimuthal direction θ and its gradient in the radial direction r is constant $\partial_r\omega_\theta(r) = 4U_b/r_0^2$. The solution of Eqs. (1) and (2) for a laminar pipe flow indicates that the generated voltage $V_{\mathrm{ISHE}}^{\mathrm{lam}}$ is a linear function of the bulk-flow velocity U_b and reads as follows:

$$\frac{r_0^3 V_{\mathrm{ISHE}}^{\mathrm{lam}}}{L} = \left(\frac{8|e|}{\hbar}\right)\left(\frac{\theta_{\mathrm{SHE}}\lambda^2\xi_{\mathrm{lam}}}{\sigma_0}\right)(U_b r_0). \tag{8}$$

The validity of Eq. (8), which has not yet been proven experimentally, is elaborated in the next section together with the results for turbulent flows at moderately high Reynolds numbers.

IV. MEASUREMENT RESULTS

A. Low-Reynolds-number laminar flows

In this section, we first present and discuss the obtained experimental results on the spin-hydrodynamic coupling at low Reynolds numbers ($20 < \mathrm{Re} < 1700$), where the flow is assumed to be fully laminar. Regardless of the flow regime, the voltage-signal measurement is carried out for a total measurement time of 10 s to avoid possible thermoelectric effects. Indeed, despite moderately high relative Seebeck coefficients of the (Ga,In)Sn and Pt electrodes $S_{(\mathrm{Ga,In})\mathrm{Sn}-\mathrm{Pt}} = +4.48\,\mu\mathrm{V\,K^{-1}}$, no significant influence of the Seebeck effect on the measured voltage V_{ISHE} is observed, as the temperatures of the top and bottom vessels remain constant during this short period of time.

Two sets of measurements are performed using narrow circular-capillary tubes with diameters of $D = 0.1$ mm and 0.4 mm to ensure that laminar flow can be established. Figure 3(a) shows, as an example, the time evolution of the voltage $V_{\mathrm{ISHE}}^{\mathrm{lam}}$ signal for different imposed pressures or pressure differences ranging from 1 bar to 6 bar. The flow is generated at $t = 0$ and ceases after 10 s. No voltage $V_{\mathrm{ISHE}}^{\mathrm{lam}} \approx 0$ is recorded until the liquid metal is driven into the capillary. As soon as the flow starts, a sharp jump is observed in the voltage signal, as can clearly be seen in Fig. 3(a). Note that the voltage signal is averaged over a shorter period of time during which the flow is steady and nonaccelerating (indicated by the vertical dashed lines). Moreover, all the reported voltages V_{ISHE} in the present study are the results of at least five individual measurements at each pressure. However, for clarity, only one signal, as an example, is plotted for each pressure in Fig. 3(a), where the generated voltage $V_{\mathrm{ISHE}}^{\mathrm{lam}}$ is obviously increased with respect to the imposed pressure or the bulk-flow velocity U_b. As said before, additional measurements in the laminar regime are carried out using a narrow capillary with a rectangular cross section to investigate the effect of the tube geometry on the spin-hydrodynamic generation. Figure 3(b) shows all the measured voltages for laminar cases with respect to the bulk-flow velocity U_b, where the minimum and maximum Reynolds numbers Re are almost 20 and 1700 for circular capillaries of $D = 0.1$ mm and 0.4 mm, respectively.

The results presented in Fig. 3(b) indicate the linear evolution of the generated voltage $V_{\mathrm{ISHE}}^{\mathrm{lam}}$ with respect to the bulk-flow velocity U_b for all investigated cases. Such behavior has been predicted by Matsuo *et al.* [15] for a laminar pipe flow with a circular cross section. However, it is interesting to see the same behavior in a rectangular capillary tube with an inhomogeneous distribution of the vorticity field across the capillary cross section. This, of course, can be explained based on the previously

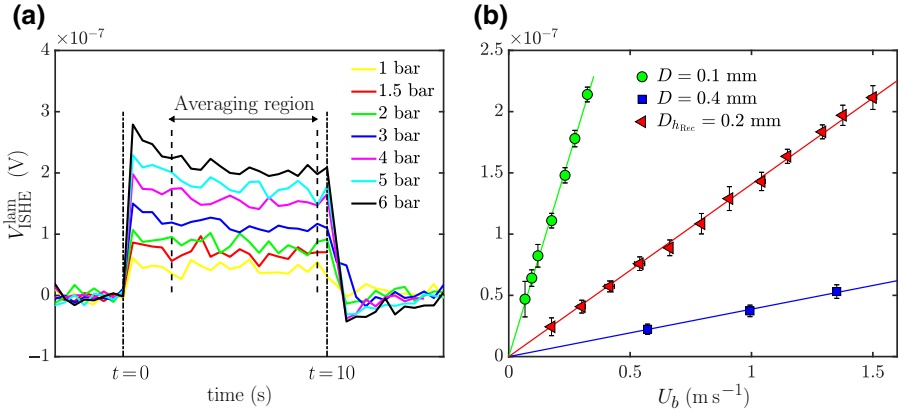

FIG. 3. The inverse spin Hall voltage $V_{\mathrm{ISHE}}^{\mathrm{lam}}$ generated by laminar flows in different capillary tubes with the same length of $L = 200$ mm. (a) The time evolution of the voltage signal $V_{\mathrm{ISHE}}^{\mathrm{lam}}$ in a circular-capillary tube with $D = 0.1$ mm where the flow is maintained for 10 s. The region between the dashed lines, in which the flow reaches steady state, is used to estimate the mean value of the generated voltage. The whole measurement interval of 10 s is indicated by the dash-dotted lines. (b) The generated voltage $V_{\mathrm{ISHE}}^{\mathrm{lam}}$ with respect to the bulk-flow velocity U_b in a circular- and a rectangular-capillary tube. The error bars show the standard deviation of at least five independent measurements.

mentioned relationship between the charge and spin current $j_i^C = -(2|e|/\hbar)\theta_{\mathrm{SHE}}\epsilon_{ijk}j_{jk}^S$, where j_{jk}^S is a second-rank tensor with nine components. Given this relationship, the longitudinal component of the induced charge current due to the ISHE in a Cartesian coordinate j_z^C should be only a result of the in-plane spin current j_{x-y}^S, i.e., $j_z^C \propto (j_{xy}^S - j_{yx}^S)$. Based on Takahashi and Maekawa [20], the spin current and consequently the charge current can be expressed as a spatial gradient of the spin voltage $j_z^C \propto (\partial\mu_y^S/\partial x - \partial\mu_x^S/\partial y)$. Using a polar coordinate system, j_z^C is reduced to $j_z^C \propto j_{r\theta}^S \propto \partial\mu_\theta^S/\partial r$ for flow in a circular pipe with only one azimuthal in-plane $(r-\theta)$ vorticity component $\omega_\theta(r)$. This allows Matsuo *et al.* [15] to analytically solve Eqs. (1) and (2) and to propose Eq. (8) as a universal scaling law. In a rectangular pipe flow, however, given the presence of two different in-plane vorticity components of $\omega_x(x,y)$ and $\omega_y(x,y)$, the calculation becomes more complicated (as it involves a series expansion of the solution) and will be reported elsewhere. Nonetheless, it is known that the in-plane vorticity components in a laminar pressure-driven flow are linearly proportional to the bulk-flow velocity $\omega_{x-y} = U_b f(x,y)$ regardless of the tube cross-sectional shape, the influence of which is represented here by $f(x,y)$ as a two-dimensional spatial function. This implies that whatever the solution of Eq. (1) for the spin-voltage field μ_{x-y}^S turns out to be, it should again be a linear function of the bulk-flow velocity, given the vorticity field $\omega_{x-y} = U_b f(x,y)$ as a source term on the right-hand side of Eq. (1). Hence, as $j_z^C \propto \nabla\mu \propto \nabla\omega$, it can be argued that the generated voltage in the laminar regime $V_{\mathrm{ISHE}}^{\mathrm{lam}}$ is linearly proportional to the bulk-flow velocity regardless of the tube cross-sectional shape.

Now, we investigate the validity of Eq. (8) for the generated voltage $V_{\mathrm{ISHE}}^{\mathrm{lam}}$ in laminar circular pipe flows. Figure 4(a) indicates all of the data points scaled based on the capillary tube radius r_0 and length L plotted versus $(U_b\, r_0)$. As can be seen, they all collapse into a single linear curve. Note that the measured voltages for the rectangular capillary tube also fall onto the same curve, utilizing the hydraulic radius $r_{h0_{\mathrm{Rec}}} = D_{h_{\mathrm{Rec}}}/2$ as the scaling parameter. However, despite this observation, we do not argue that the hydraulic radius $r_{h0_{\mathrm{Rec}}}$ is a universal parameter for scaling the generated voltage $V_{\mathrm{ISHE}}^{\mathrm{lam}}$ in a capillary tube with a noncircular cross section. As discussed above, to propose a universal scaling, the general solution of Eq. (1) should be provided for a capillary tube with an arbitrary cross section.

It is also interesting to have a look at the similarity between Eq. (8) and the well-known correlation for the pressure drop in a laminar pressure-driven flow, which reads

$$\Delta p = f_{\mathrm{lam}}\frac{L}{D}\frac{\rho U_b^2}{2}. \tag{9}$$

Using the friction factor for a laminar flow $f_{\mathrm{lam}} = 64/\mathrm{Re}$, the pressure-drop correlation can be reformulated as follows:

$$\frac{r_0^3\Delta p}{L} = 8\mu(U_b\, r_0), \tag{10}$$

where μ is the dynamic viscosity of the fluid. From the similarity between Eqs. (8) and (10), it is possible to relate the generated voltage to the pressure drop of a laminar flow as follows:

$$V_{\mathrm{ISHE}}^{\mathrm{lam}} = \left(\frac{|e|}{\hbar}\right)\left(\frac{\theta_{\mathrm{SHE}}\lambda^2\xi_{\mathrm{lam}}}{\mu\sigma_0}\right)\Delta p. \tag{11}$$

The above equation shows that using the same working liquid, the generated voltage $V_{\mathrm{ISHE}}^{\mathrm{lam}}$ should be the same at the same imposed pressure even for capillary tubes with different lengths and diameters. Figure 4(b) shows the generated voltages $V_{\mathrm{ISHE}}^{\mathrm{lam}}$ versus the pressure drop Δp, i.e., the imposed pressure, in the circular- and the rectangular-capillary tubes. As can be seen, the same voltage is obtained for all cases at the same imposed pressure. However, it should be noted that the validity of Eq. (11) relies on the reliability of the friction-factor correlation for a laminar flow f_{lam}. While $f_{\mathrm{lam}} = 64/\mathrm{Re}$ is a very well-accepted correlation for circular tubes, it has been shown that it results in a significant uncertainty (around $\pm 40\%$) in estimating the pressure drop based on the hydraulic diameter D_h in noncircular tubes [14]. Nonetheless, the voltages measured here for the rectangular capillary tube again show a consistency with other data and Eq. (11). The proposed correlation in Eq. (11) may have implications for the design of small-scale electric generators based on spin-hydrodynamic coupling.

B. High-Reynolds-number turbulent flows

Measurements are also performed for turbulent flows in circular-capillary tubes with different diameters of $D = 0.4$, 0.8, and 1.2 mm. Figure 5(a) shows the measured voltage V_{ISHE} for a $D = 0.4$ mm capillary tube with respect to the Reynolds number $700 < \mathrm{Re} < 3200$, where both the laminar and the turbulent regimes are covered. Here, the transition from laminar to turbulent can be clearly identified from the measured voltages V_{ISHE}, where it increases linearly in the laminar regime $\mathrm{Re} < 2000$ and nonlinearly in the fully turbulent $\mathrm{Re} > 2500$ regime, with the critical transition Re being about 2300. As discussed before, the nonlinear behavior of the voltage with respect to the turbulent friction velocity u_τ, which is itself a nonlinear function of the Reynolds number Re, has been predicted and verified by Takahashi *et al.* [10] using Hg as the working liquid [see Eq. (6)]. These authors have also reported a measurement in which they used (Ga,In)Sn as the working liquid. In the present study, the data points provided

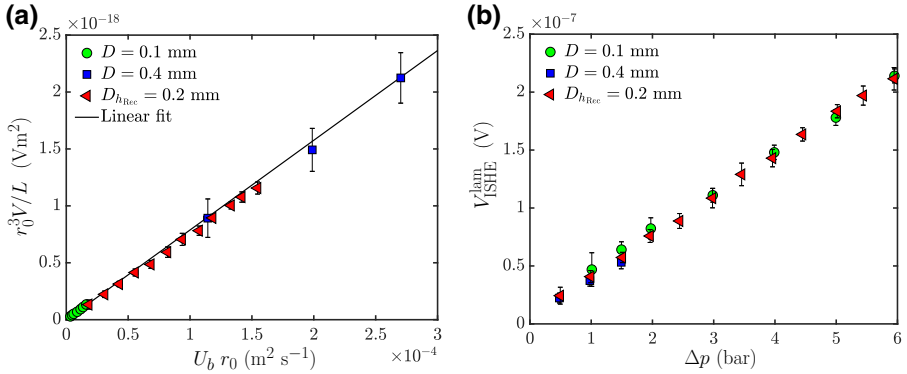

FIG. 4. The voltage $V_{\mathrm{ISHE}}^{\mathrm{lam}}$ generated by laminar flows, (a) scaled based on Eq. (8) versus $(U_b\, r_0)$ and (b) with respect to the imposed pressure Δp [see Eq. (10)].

in Fig. 3(b) of Takahashi *et al.* [10] are extracted and used to verify the measurements for the turbulent regime. Figure 5(b) shows the extracted data points (light blue pentagrams) together with our measured voltages, which are scaled based on $r_0^3 V/L$ and plotted versus $u_\tau r_0$. Here, $u_\tau = \sqrt{\tau_w/\rho}$ and the wall-shear stress $\tau_w = C_f\, \rho U_b^2/2$ are estimated based on the measured bulk-flow velocity U_b and the well-known Blasius correlation for the friction factor $C_f = 0.0791\mathrm{Re}^{-0.25}$ for a turbulent circular pipe flow [21]. As can be seen from Fig. 5(b), the nonlinear fit to the measured data points (black solid line) based on Eq. (6) overlaps nicely with the fit generated from the extracted data points (light blue dashed line). Indeed, the maximum Reynolds number achieved by Takahashi *et al.* [10] could be estimated based on their pipe diameter $D = 0.4$ mm to be around $\mathrm{Re} \approx 5000$. Here, we reach a significantly higher Reynolds number of $\mathrm{Re} = 2.1 \times 10^4$ using a capillary tube with a diameter of $D = 1.2$ mm. These results show that the proposed universal scaling law by Takahashi *et al.* [10] describes the spin hydrodynamic phenomenon very well even at very high Reynolds numbers.

We also calculate the constant coefficients of the fitted curves presented in Figs. 4(b) and 5(b) for the scaling laws of the spin-hydrodynamic coupling for laminar and turbulent flows. Based on Eqs. (6) and (8), these constants can be expressed as $C_{\mathrm{lam}} = (8|e|/\hbar)[(\theta_{\mathrm{SHE}}\lambda^2\xi_{\mathrm{lam}})/\sigma_0] = 7.88 \times 10^{-15}$ (Vs) and $C_{\mathrm{turb}} = (4|e|/\hbar)[(\theta_{\mathrm{SHE}}\lambda^2\xi_{\mathrm{turb}})/\sigma_0](1/\kappa_+) = 1.53 \times 10^{-14}$ (Vs) for laminar and turbulent flow, respectively. Note that except for ξ_{lam} and ξ_{turb}, all the parameters in C_{lam} and C_{turb} are considered to be independent of the flow. Hence, the ratio between ξ_{lam} and ξ_{turb} can be obtained as $\xi_{\mathrm{turb}}/\xi_{\mathrm{lam}} = 1.60$.

Finally, we briefly discuss the possibility that the generated electric voltage could be the result of a dynamo effect in the electrically conducting fluid flow. In magnetohydrodynamics, the dynamics of the magnetic field **B** is given by the induction equation [22]:

$$\frac{\partial \mathbf{B}}{\partial t} = \nabla \times (\mathbf{u} \times \mathbf{B}) + \beta \nabla^2 \mathbf{B}, \tag{12}$$

where β is the magnetic diffusivity. The dimensionless magnetic Reynolds number R_m relates the magnitudes of both terms on the right-hand side of Eq. (12) to each other. In detail, $R_m = \mathrm{Re}\,\mathrm{Pr}_m$, where $\mathrm{Pr}_m = \nu/\beta$ is known as the magnetic Prandtl number. It has been proven rigorously that for a velocity field to generate a dynamo, a certain principal rate of strain (or mean shear rate) is necessary such that the total magnetic energy $M(t) = 1/(2\mu_0) \int_V \mathbf{B}^2 dV$ over the whole space V (with μ_0 being the permeability of free space) does not decay to zero with respect to time (see Moffatt [23]). This inequality, which follows from the energy balance in the magnetohydrodynamic flow, can be translated into a critical magnetic Reynolds number above which a dynamo sets in, $R_m^* = \pi^2$ [23]. In the present study, however, due to the low

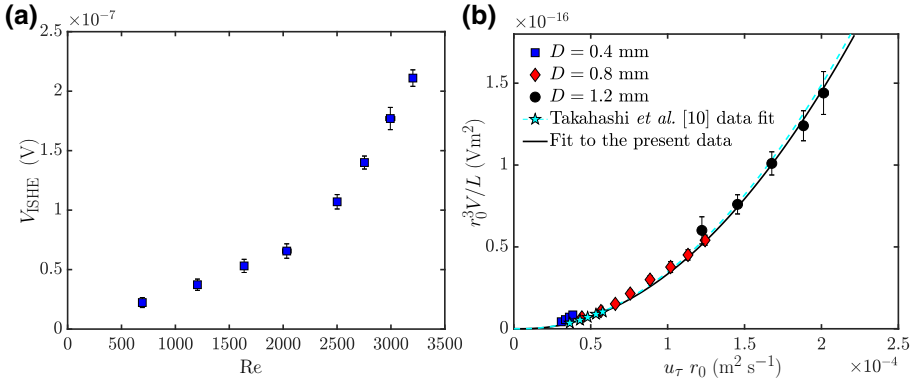

FIG. 5. (a) The generated voltage V_{ISHE} versus the Reynolds number Re using a capillary tube of circular cross section with $D = 0.4$ mm. (b) Scaling of the generated voltage $V_{\mathrm{ISHE}}^{\mathrm{turb}}$ by turbulent flows with respect to $u_\tau r_0$ [see Eq. (6)].

magnetic Prandtl number of (Ga,In)Sn, $\mathrm{Pr}_m = 1.37 \times 10^{-6}$ (see Table I), the magnetic Reynolds number is limited to $R_m \lesssim 3 \times 10^{-2} \ll R_m^*$ for the range of the flow Reynolds number Re under investigation. This value is at least 3 orders of magnitude smaller than the well-accepted critical R_m for the onset of dynamo action. The existence of a critical $R_m > 10$ for triggering dynamo action in turbulent liquid-metal flows is also supported by recent large-scale laboratory experiments using specific flow patterns (for reviews, see Refs. [24,25]). Furthermore, it is believed that a nonvanishing flow helicity $H(t) = \int_V (\mathbf{u} \cdot \boldsymbol{\omega})\, dV$ is required in addition for a dynamo to act [22]. We emphasize that a laminar flow through a straight pipe, which is shown to generate an electric voltage for $\mathrm{Re} \gtrsim 20$, has zero helicity. Hence, it can be concluded that the measured nanovoltage in the present study is not the result of a dynamo-generated magnetic field in combination with a classical Hall effect.

V. CONCLUSIONS AND DISCUSSION

We present liquid-metal pipe-flow experiments in a narrow capillary that generates a measurable nanovoltage caused by the collective coupling of the spins of the freely moving electrons to the macroscopic vorticity of the charged fluid. We extend the original experiments by Takahashi *et al.* [10] in both directions with respect to the Reynolds number of the pipe flow: (1) to the laminar regime, where a linear scaling of the generated electric voltage to the bulk-flow velocity U_b holds; and (2) to higher Reynolds numbers with a fully developed turbulent circular pipe flow, where the predicted scaling with respect to the turbulent friction velocity u_τ is found to continue to exist. We also vary the geometry of the capillary to that of a rectangular cross section and demonstrate the robustness of the laminar scaling.

Our presented experiments are an independent confirmation and extension of the work of Takahashi *et al.* [10], which demonstrates spin-hydrodynamic generation without external magnetic fields, a method of electricity generation by a coupling of spintronics with fluid dynamics. Even though the qualitative scaling behavior seems to be geometry independent, our studies indicate the potential of an optimization of the voltage generation in several ways. In our view, the detection of the linear dependence of the spin voltage on the Reynolds number in the laminar-regime provides an interesting starting point, as it will make the setup accessible to further microfluidic analysis at low Reynolds numbers in the future. This includes, besides analytical calculations and the variation of the cross section geometry, such as different ducts and elliptical pipes, the application of nanostructured walls and/or Dean flow geometries to further maximize the magnitude of the vorticity gradient in laminar flows. The latter can result in a stronger coupling to the electron spin dynamics and thus generate a higher spin voltage without the large pressure drops that are necessary for turbulent flows. These studies are currently under way and will be reported elsewhere.

ACKNOWLEDGMENTS

This work was financially supported by the Volkswagen Foundation. We are grateful to Christian Resagk, Till Zürner, Thomas Boeck, Frank Stefani, and Yuri Kolesnikov for fruitful discussions, comments, and remarks.

[1] W. F. Vinen and R. J. Donnelly, Quantum turbulence, Phys. Today **60**, 43 (2007).
[2] E. Fonda, K. R. Sreenivasan, and D. P. Lathrop, Reconnection scaling in quantum fluids, Proc. Natl. Acad. Sci. USA **116**, 1924 (2019).
[3] L. Levitov and G. Falkovich, Electron viscosity, current vortices and negative nonlocal resistance in graphene, Nat. Phys. **12**, 672 (2016).
[4] S. Wolf, D. Awschalom, R. Buhrman, J. Daughton, S. Von Molnar, M. Roukes, A. Y. Chtchelkanova, and D. Treger, Spintronics: A spin-based electronics vision for the future, Science **294**, 1488 (2001).
[5] I. Žutić, J. Fabian, and S. D. Sarma, Spintronics: Fundamentals and applications, Rev. Mod. Phys. **76**, 323 (2004).
[6] A. Hirohata and K. Takanashi, Future perspectives for spintronic devices, J. Phys. D. Appl. Phys. **47**, 193001 (2014).
[7] K. Ando, M. Morikawa, T. Trypiniotis, Y. Fujikawa, C. Barnes, and E. Saitoh, Direct conversion of light-polarization information into electric voltage using photoinduced inverse spin-Hall effect in Pt/GaAs hybrid structure: Spin photodetector, J. Appl. Phys. **107**, 113902 (2010).
[8] C. W. Sandweg, Y. Kajiwara, A. V. Chumak, A. A. Serga, V. I. Vasyuchka, M. B. Jungfleisch, E. Saitoh, and B. Hillebrands, Spin Pumping by Parametrically Excited Exchange Magnons, Phys. Rev. Lett. **106**, 216601 (2011).
[9] K. Uchida, S. Takahashi, K. Harii, J. Ieda, W. Koshibae, K. Ando, S. Maekawa, and E. Saitoh, Observation of the spin Seebeck effect, Nature **455**, 778 (2008).
[10] R. Takahashi, M. Matsuo, M. Ono, K. Harii, H. Chudo, S. Okayasu, J. Ieda, S. Takahashi, S. Maekawa, and E. Saitoh, Spin hydrodynamic generation, Nat. Phys. **12**, 52 (2016).
[11] M. Matsuo, J. Ieda, K. Harii, E. Saitoh, and S. Maekawa, Mechanical generation of spin current by spin-rotation coupling, Phys. Rev. B **87**, 180402 (2013).
[12] J. Sinova, S. O. Valenzuela, J. Wunderlich, C. Back, and T. Jungwirth, Spin Hall effects, Rev. Mod. Phys. **87**, 1213 (2015).
[13] E. Saitoh, M. Ueda, H. Miyajima, and G. Tatara, Conversion of spin current into charge current at room temperature: Inverse spin-Hall effect, Appl. Phys. Lett. **88**, 182509 (2006).
[14] F. M. White, *Fluid Mechanics* (McGraw-Hill, New York, 2015).

[15] M. Matsuo, Y. Ohnuma, and S. Maekawa, Theory of spin hydrodynamic generation, Phys. Rev. B **96**, 020401 (2017).
[16] Y. Plevachuk, V. Sklyarchuk, S. Eckert, G. Gerbeth, and R. Novakovic, Thermophysical properties of the liquid Ga-In-Sn eutectic alloy, J. Chem. Eng. Data **59**, 757 (2014).
[17] S. Eckert, Private communication.
[18] T. Valet and A. Fert, Theory of the perpendicular magnetoresistance in magnetic multilayers, Phys. Rev. B **48**, 7099 (1993).
[19] S. B. Pope, *Turbulent Flows* (Cambridge University Press, Cambridge, England, 2001).
[20] S. Takahashi and S. Maekawa, Spin current, spin accumulation and spin Hall effect, Sci. Technol. Adv. Mat. **9**, 014105 (2008).
[21] J. Eggels, F. Unger, M. Weiss, J. Westerweel, R. Adrian, R. Friedrich, and F. Nieuwstadt, Fully developed turbulent pipe flow: A comparison between direct numerical simulation and experiment, J. Fluid Mech. **268**, 175 (1994).
[22] P. A. Davidson, *An Introduction to Magnetohydrodynamics* (Cambridge University Press, Cambridge, England, 2001).
[23] H. K. Moffatt, *Magnetic Field Generation in Electrically Conducting Fluids* (Cambridge University Press, Cambridge, England, 1978).
[24] A. Gailitis, O. Lielausis, E. Platacis, G. Gerbeth, and F. Stefani, Colloquium: Laboratory experiments in hydromagnetic dynamos, Rev. Mod. Phys. **74**, 973 (2002).
[25] A. Gailitis, G. Gerbeth, T. Gundrum, O. Lielausis, G. Lipsbergs, E. Platacis, and F. Stefani, Self-excitation in a helical liquid metal flow: The Riga dynamo experiments, J. Plasma Phys. **84**, 735840301 (2018).